from a higher D-A blend phase separation and lower homogeneity in the vertical direction (**Figure 4a,** P3HT enrichment of the top regions and $IC_{70}BA$#1 settlement at the bottom of the layer). The lowest device characteristics were observed when no SA and no TA was carried out, with a measured average J_{SC} and PCE of 4.83 ± 0.18 mA cm^{-2} and 1.42 ± 0.12%. This is due to lower light absorption and less self-organization and crystallization of the P3HT:$IC_{70}BA$#1 blend evident from the UV-vis characterization. We believe that these adverse device characteristics have a direct connection with the disadvantageous molecular packing of $IC_{70}BA$#1, which originates from the fact that without SA and TA, there is insufficient time and temperature for rearrangement and slow melting of the $IC_{70}BA$#1 regio-isomers, in order to form an appropriate BHJ morphology and improve the exciton separation yields and free charge transfer processes.

To tune the BHJ thickness, P3HT:$IC_{70}BA$#1 PSCs produced from 40, 42, and 45 mg mL^{-1} solutions were characterized as shown in Figure S18 and summarized in Table S3. In addition, to achieve the optimal device characteristics, the spin-coating speed for the P3HT:$IC_{70}BA$#1 layer was altered from 500 to 850 rpm (Figure S19, Table S4). Interestingly, there is a continuous decrease of the J_{SC} values, related to the BHJ thickness (Figure S12), from 10.05 mA cm^{-2} (Figure S19a; 500 rpm devices; thickness of 238.3 nm ± 3.86 nm) down to 6.10 mA cm^{-2} (Figure S19b; 850 rpm devices; thickness of 175.3 nm ± 4.11 nm). Based on the UV-vis data in **Figure 3b**, we summarize that this J_{SC} decrease, is dominated by the rapid drying of the P3HT:$IC_{70}BA$#1 layer during the spin-coating process, leading to reduced film crystallinity and unbalanced vertical D-A material distribution. This additionally lowers the FF and PCE for the 850 rpm devices (55.75% and 2.98%), when compared to the other PSCs. The highest average PCE values of 5.97 ± 0.40% and 5.95 ± 0.29% were measured for devices fabricated at 600 and 650 rpm, respectively. This originates form a balanced charge carrier transport as evidenced by the high average FF values of 69.7% and 71.3%, respectively. The best performing P3HT:$IC_{70}BA$#1 device exhibits V_{OC} of 0.86 eV, J_{SC} of

10.91 mA cm^{-2}, and a FF of 72%, leading to a peak PCE of 6.74%. It is worth noting, that this PCE value represents a record PCE measured for such large device active area (0.43 cm^2), when compared to average reported PCEs of approx. 4.5% for devices areas less than 0.1 cm^2, respectively.

To test the importance of the regio-isomeric mixture of $IC_{70}BA$ on the molecular packing of the BHJ and hence device PCE, we applied the tailored fabrication conditions found for $IC_{70}BA$#1 (5, 2, and 12 o'clock regio-isomers with a distribution of 22%, 43%, and 35%, see Figure S1 and Table S1), onto $IC_{70}BA$#2, which exhibits a different 5, 2, and 12 o'clock regio-isomeric distribution (16%, 36%, and 48%, see Figure S2 and Table S2). **Figure 6a** and Table 1 show the comparison of the best performing device from each $IC_{70}BA$ batch, fabricated under identical conditions.

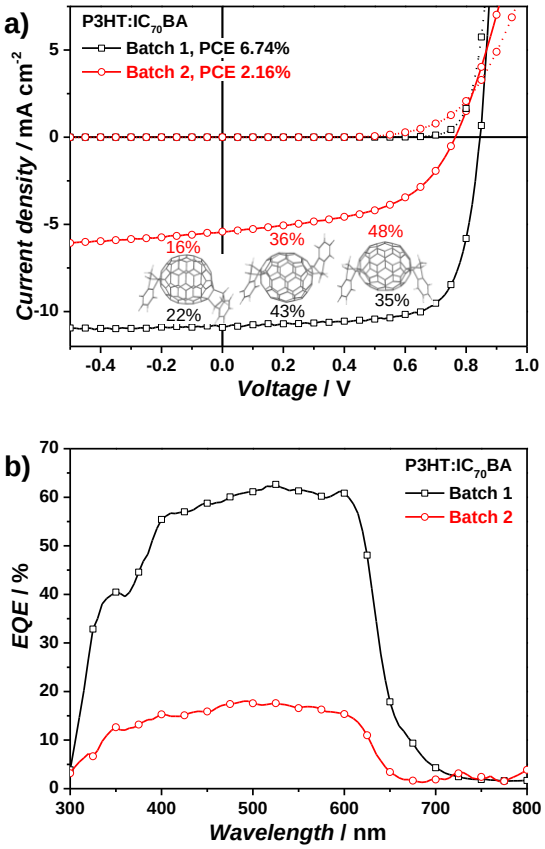

Figure 6. (a) J-V characteristics of P3HT:$IC_{70}BA$ PSCs under illumination of AM1.5G (100 mW cm^{-2}) (solid lines) and in the dark (dotted lines) for two different $IC_{70}BA$ batches. (b) corresponding EQE spectra.

It is known that BHJ blends of the 2 o'clock regio-isomer in combination with P3HT deliver the highest device PCE.[36] This is supported by the fact that the 2 o'clock regio-isomer exhibits the shortest distance between the "pole" carbon atom and the indene addend at the opposite pole (8.36 Å, Figure S6), which can be related to reduced hopping distances and improved electron conduction due to closely packed fullerene-fullerene molecules improving the electron mobility and carrier transport properties.[10, 54] However, based on our results for $IC_{70}BA$#1 shown in **Figure 5a**, comparable high PCEs are also possible for a mixture of $IC_{70}BA$ regio-isomers, if a predominantly 2 o'clock regio-isomeric content is present, and appropriate device fabrication conditions are used. Yet, the ratio of the remaining regio-isomer distribution needs to be considered and can be crucial for the device performance. As shown in **Figure 6a**, despite a close 2 o'clock distribution for the $IC_{70}BA$#1 and $IC_{70}BA$#2 (43% *vs.* 36%), a variation of the 5 and 12 o'clock regio-isomer ratio (22% and 35% *vs.* 16% and 48%) is sufficient to reduce the device J_{SC} and PCE from 10.91 mA cm^{-2} and 6.74% to 5.42 mA cm^{-2} and 2.16%. It should be noted that $IC_{70}BA$#2 exhibits a significantly larger amount of the 12 o'clock regio-isomer. It is believed that the highly symmetric nature of the indene addends for the 12 o'clock regio-isomer impedes the π-π stacking of the P3HT molecules, due to high crystallite formation within the regio-isomeric molecules, disturbing the intermolecular ordering and charge transfer properties of the donor phase. This, on the other hand, can directly related to a reduced charge carrier mobilities and exciton dissociation yields, lowering the device J_{SC}, FF, and PCE.[10, 54] These assumptions are additionally supported by the observations made for the isolated 12 o'clock regio-isomer, which was visibly less soluble, and solutions were less stable, and prone to larger cluster aggregation, compared to the other regio-isomers.

To ensure that the J_{SC} measured under irradiation by the solar simulator is within an acceptable error, we also measured the external quantum efficiency (EQE) spectra for the devices (**Figure 5b** and **6b**). It can be seen in **Figure 5b** that the corresponding EQE spectra

of devices with a P3HT:$IC_{70}BA$#1 BHJ subjected to SA and TA reach about 60% for the wavelengths 450 – 600 nm. Slightly lower EQE values were measured for SA only BHJs. Layers fabricated with TA only or without any annealing step show the lowest EQE values pointing to strongly reduced exciton dissociation rates and charge carrier transport processes. This assumption is further strengthened after comparison with the EQE spectra between $IC_{70}BA$#1 and $IC_{70}BA$#2, shown in **Figure 6b**, where an EQE of only about 15% was measured for the devices fabricated with $IC_{70}BA$#2.

3. Conclusion

For this study, we show a thorough characterization of commercial $IC_{70}BA$ samples. After conducting HPLC, UV-vis, ^{1}H NMR, and ^{13}C NMR characterization of two different $IC_{70}BA$ batches, we found different isomeric distributions of the 2, 5, and 12 o'clock regio-isomers within each batch. In a case study investigating the thermal stability and phase transition properties of $IC_{70}BA$ batch#1 and in its blend with P3HT, we postulate the presence of morphological changes in the D-A blend, altering the phase separation of the BHJ. To the best of our knowledge, we are the first to report the use of SE as a non-destructive characterization technique to investigate the volume fraction distribution of P3HT and $IC_{70}BA$ blends. Taking the data from the SE in conjunction with UV-vis, TGA, DSC, and AFM data, we demonstrate that there is a difference in the crystallization transformation of the blend between P3HT and the regio-isomeric mixture of $IC_{70}BA$ depending on the fabrication process used. This affects the molecular packing of the photoactive layer and therefore the device PCE. Based on these findings, we have determined the optimal fabrication conditions for the production of P3HT:$IC_{70}BA$ PSCs with PCEs above 6.7% for a particular regio-isomeric distribution. The sensitivity of the spatial molecular packing of BHJs between donor materials and isomeric fullerene acceptors is illustrated with different isomeric fractions of $IC_{70}BA$. As such, we demonstrate how the PSC characteristics can be improved in the future based on an

understanding of the formation kinetics of the BHJ phase separation, which allows for the fabrication of highly efficient PCSs.

We also show that despite a high $IC_{70}BA$ material purity of above 99% for different material batches, the crucial factor determining the PCE is the variation of the regio-isomeric ratio of $IC_{70}BA$ when blended with P3HT. The device performance can be optimized after tailoring the regio-isomeric ratio in the mixture or utilizing individual $IC_{70}BA$ isomers, which is currently under investigation. The outcomes of this study provide a better understanding of the D-A phase formation and separation, and pave the way towards a fundamental understanding of the spatial molecular packing of numerous BHJ materials systems (including ternary BHJs), in which fullerene derivatives with isomeric properties are used as electron accepting materials.

4. Experimental Section

Materials: Regioregular poly(3-hexylthiophene) (P3HT 4002-EE, Rieke Metals Inc.) and indene-C_{70}-bisadduct ($IC_{70}BA$, 1-Material – Organic Nano Electronic) were used as the D-A components in a solution of 1,2-dichlorobenzene (o-DCB, 99%). Poly(3,4-ethylenedioxythiophene) poly-(styrene sulfonate) (PEDOT-PSS Clevios P VP AI 4083, Heraeus Holding GmbH) was used as the hole transport layer and 2,9-dimethyl-4,7-diphenyl-1,10-phenanthroline (BCP or bathocuproine, Luminescence Technology Corp.) was used as the electron transport layer.

Device fabrication: Pre-patterned glass substrates (15 Ω sq^{-1}., Luminescence Technology Corp.) were sonicated sequentially in decon 90 water, deionized (DI) water, acetone and methanol for 5 min each, followed by an oxygen plasma treatment (5 min, 100 W, 15 sccm O_2, Emitech K1050X plasma cleaner). PEDOT:PSS films were produced by spin-coating (60 s at 4000 rpm) from a filtered solution under ambient conditions, and subsequently annealed for

30 min at 150 °C. Equal material weight concentrations of P3HT and $IC_{70}BA$ (20, 21 or 22.5 mg) were mixed into o-DCB (1 mL, 1:1 ratio) and dissolved for at least 24 hours under vigorous stirring at room temperature. The P3HT:$IC_{70}BA$ solution was then spin-coated on top of the PEDOT:PSS film, initially for 80 s at speed of 500 - 850 rpm, followed by a second step for 5 s at 1000 rpm. The wet film was either allowed to quick dry in approx. 5 s under inert atmosphere conditions at room temperature, or was covered with a petri dish (60 mm diameter, 15 mm height) for 30 min to enable slow drying of the film. Thermal annealing (10 min, 90 - 50 °C) was also carried out when required. For PSC device fabrication, BCP (2-3 nm) and aluminium (75 nm) were evaporated through a shadow mask, at pressures below 3 x 10^{-6} mbar. The Al/ITO electrodes overlap within the devices was 0.90 cm^2. All fabrication steps after the PEDOT:PSS deposition were performed in a nitrogen-filled glove box.

Solid films characterization: Optical characterization (Varian Cary 5000 UV-vis-NIR spectrophotometer) was undertaken relative to a glass reference in the wavelength range 300 - 900 nm (scan rate 600 nm min^{-1} and a sampling interval of 1 nm). Film thickness measurements were conducted using a Dektak 8 profilometer. Surface topography characterization was performed using a Veeco Dimension 3000 AFM system in tapping mode on 3 different locations on the sample surface. Thermogravimetric analysis (TGA, TA Q500 thermogravimetric analyser) was conducted from room temperature (27 °C) to 800 °C or 900 °C with a heating rate of 10 °C min^{-1} and a N_2 sample purge flow (60 mL min^{-1}). Differential scanning calorimetry (DSC, TA Q1000 DSC) was undertaken using aluminium weighing pans, with heating and cooling rates of 10 °C min^{-1} and a N_2 purge flow (50 mL min^{-1}).

$IC_{70}BA$ characterization: High performance liquid chromatography (HPLC) spectra were obtained on a Japan Analytical Industry (JAI) LC-9103 Recycling Preparative HPLC with a

modular Hitachi L-7150 pump and JAI UV Detector 3702. The following parameters were used: Cosmosil® Buckyprep-M 20.0 mm ID x 250 mm column, toluene solvent, 16 ml min^{-1} flow rate, and 312 nm absorption. Mass spectra (MS) of the fractions were obtained on a Bruker microflex™ LT using matrix-assisted laser desorption/ionization time-of-flight mass spectrometry (MALDI-TOF MS) analysis. Negative ionization was employed and trans-2-[3-(4-t-butyl-phenyl)-2-methyl-2-propenylidene] malononitrile (DCTB) was used as the matrix material. UV-vis spectra of the fractions, isolated by HPLC, were obtained on a Jasco V-570 Spectrophotometer in toluene. Samples for proton nuclear magnetic resonance (^{1}H NMR) spectroscopy were dried in vacuo for at least 24 hours before being dissolved in deuterated chloroform (CDCl3). All spectra were obtained on a 400 MHz Bruker AVIII400 spectrometer. The optical properties and the morphology of the P3HT:$IC_{70}BA$#1 samples (two sets of samples) have further been investigated using a phase modulated Spectroscopic Ellipsometer (Horiba) from near infrared to far UV (0.7–6.5 eV) with steps of 20 meV with 70° angle of incidence. The optical response of the substrate layers (glass and ITO) was measured followed by the measurement and calculation of the optical properties of pristine P3HT and $IC_{70}BA$ materials (see S7 in Supplementary Information) was performed in order to be used as reference for the analysis of the $<\varepsilon(\omega)>$ of the P3HT:$IC_{70}BA$ blends. Contact angle (CA) measurements (CAM 200, KSV Instruments Ltd.) were conducted using a static drop technique with a deionized (DI) water droplet (5 µl) and a surface tension of 72.8 mN m^{-1}. Surface energies were calculated using the relation reported by Chibowski et al.[55]. Cyclic voltammograms of P3HT:$IC_{70}BA$ blend films deposited onto ITO electrodes were performed in 0.1 M NBu_4PF_6/MeCN and 0.1 M $NHex_4PF_6$/MeCN in a gas tight three electrode cell (counter electrode: Pt plate; pseudo-reference electrode: Ag wire coated with an AgCl layer, directly immersed into the electrolyte solution) under argon atmosphere at room temperature. The I-E curves were recorded with a scan rate of 20 mV s^{-1}. Oxidation and reduction potential cycles were recorded separately. For the calculation of the LUMO and HOMO energy values

the half wave potential ($E_{1/2}$) of the first fullerene reduction and the onset potential of the P3HT oxidation (p-doping) was used, respectively. Energy levels were calculated assuming that the Fc/Fc^+ couple is located at -5.1 eV in the Fermi scale.[56]

Device characterization: Current-voltage (I-V) characterization was conducted in ambient atmosphere, without encapsulation, using a four-point probe configuration (Keithley 2400 source measurement apparatus). An Abet Technologies 10500 solar simulator (class AAB) at AM 1.5 G, calibrated with a silicon reference cell (PV Measurements, Inc. 20 x 20 mm) to 100 mW cm^{-2}, was used to illuminate the devices. For more accurate definition of the illuminated area, an aperture of 0.43 cm^2 was used. For external quantum efficiency (EQE) measurements, a Bentham Instruments PVE 300, with 1-Sun light bias, was utilized in the wavelength range from 300 nm to 800 nm (5 nm step).

Supporting Information
Supporting Information is available from the Wiley Online Library or from the author.

Acknowledgements
The authors would like to acknowledge Dr Edward New, Dr K. D. G. Imalka Jayawardena, Dr Adrian Ruff, Dr Michail Terzidis and Dr Ian Hamerton for fruitful discussions and Violeta Doukova for conducting the TGA and DSC characterization. We gratefully acknowledge support received from the European Commission 7th framework programme SMARTONICS (Grant Agreement Number 310229).

Received: ((will be filled in by the editorial staff))
Revised: ((will be filled in by the editorial staff))
Published online: ((will be filled in by the editorial staff))

[1] J.-D. Chen, C. Cui, Y.-Q. Li, L. Zhou, Q.-D. Ou, C. Li, Y. Li and J.-X. Tang, *Adv. Mater.* **2015**, *27*, 1035.

[2] J. Huang, J. H. Carpenter, C.-Z. Li, J.-S. Yu, H. Ade and A. K.-Y. Jen, *Adv. Mater.* **2016**, *28*, 967.

[3] Z. Zheng, S. Zhang, J. Zhang, Y. Qin, W. Li, R. Yu, Z. Wie and J. Hou, *Adv. Mater.* **2016**, *28*, 5133.

[4] Q. Wan, X. Guo, Z. Wang, W. Li, B. Guo, W. Ma, M. Zhang and Y. Li, *Adv. Funct. Mater.* **2016**, *26*, 6635.

[5] K. D. G. I. Jayawardena, L. J. Rozanski, C. A. Mills and S. R. P. Silva, *Nat. Photon.* **2015**, *9*, 207.

[6] M. J. Beliatis, K. K. Gandhi, L. J. Rozanski, R. Rhodes, L. McCafferty, M. R. Alenezi, A. S. Alshammari, C. A. Mills, K. D. G. I. Jayawardena, S. J. Henley and S. R. P. Silva, *Adv. Mater.* **2013**, *26*, 2078.

[7] N. Li, P. Kubis, K. Forberich, T. Ameri, F. C. Krebs and C. J. Brabec, *Sol. Energy Mater. Sol. Cells* **2013**, *120*, 701.

[8] L. Lucera, F. Machui, P. Kubis, H. D. Schmidt, J. Adams, S. Strohm, T. Ahmad, K. Forberich, H.-J. Egelhaaf and C. J. Brabec, *Energy Environ. Sci.* **2016**, *9*, 89.

[9] Y. Zhang, J. Griffin, N. W. Scarratt, T. Wang and D. G. Lidzey, *Prog. Photovolt: Res. Appl.* **2016**, *24*, 275.

[10] H. K. H. Lee, Z. Li, I. Constantinou, F. So, S. W. Tsang and S. K. So, *Adv. Energy Mater.* **2014**, *4*, 1614.

[11] K. Tremel and S. Ludwigs, in *Advances in Polymer Science*, S. Ludwigs, Springer Berlin Heidelberg, **2014**, *265*, 39.

[12] Y. Kim, S. Cook, S. M. Tuladhar, S. A. Choulis, J. Nelson, J. R. Durrant, D. D. C. Bradley, M. Giles, I. McCulloch, C.-S. Ha and M. Ree, *Nat. Mater.* **2006**, *5*, 197.

[13] J. E. Carlé, T. R. Andersen, M. Helgesen, E. Bundgaard, M. Jørgensen and F. C. Krebs, *Sol. Energy Mater. Sol. Cells* **2013**, *108*, 126.

[14] J. Y. Oh, M. Shin, T. I. Lee, W. S. Jang, Y.-J. Lee, C. S. Kim, J.-W. Kang, J.-M. Myoung, H. K. Baik and U. Jeong, *Macromolecules* **2013**, *46*, 3534.

[15] M. T. Dang, L. Hirsch, G. Wantz and J. D. Wuest, *Chem. Rev.* **2013**, *113*, 3734.

[16] Z. Xu, L.-M. Chen, G. Yang, C.-H. Huang, J. Hou, Y. Wu, G. Li, C.-S. Hsu and Y. Yang, *Adv. Funct. Mater.* **2009**, *19*, 1227.

[17] Z. Hu, J. Zhang and Y. Zhu, *Appl. Phys. Lett.* **2013**, *102*, 043307.

[18] G. Li, V. Shrotriya, J. Huang, Y. Yao, T. Moriarty, K. Emery and Y. Yang, *Nat. Mater.* **2005**, *4*, 864.

[19] W. Ma, C. Yang, X. Gong, K. Lee and A. J. Heeger, *Adv. Funct. Mater.* **2005**, *15*, 1617.

[20] M. C. Scharber, D. Muehlbacher, M. Koppe, P. Denk, C. Waldauf, A. J. Heeger and C. J. Brabec, *Adv. Mater.* **2006**, *18*, 789.

[21] M. T. Dang, L. Hirsch and G. Wantz, *Adv. Mater.* **2011**, *23*, 3597.

[22] L. J. A. Koster, V. D. Mihailetchi and P. W. M. Blom, *Appl. Phys. Lett.* **2006**, *88*, 093511.

[23] Y. He and Y. Li, *Phys. Chem. Chem. Phys.* **2011**, *13*, 1970.

[24] Y. He, G. Zhao, B. Peng and Y. Li, *Adv. Funct. Mater.* **2010**, *20*, 3383.

[25] Y. He, H.-Y. Chen, J. Hou and Y. Li, *J. Am. Chem. Soc.* **2010**, *132*, 1377.

[26] D. Angmo, M. Bjerring, N. C. Nielsen, B. C. Thompson and F. C. Krebs, *J. Mater. Chem. C* **2015**, *3*, 5541.

[27] X. Fan, S. Li, S. Guo and G. Fang, *J. Phys. D: Appl. Phys.* **2013**, *46*, 055502.

[28] X. Guo, C. Cui, M. Zhang, L. Huo, Y. Huang, J. Hou and Y. Li, *Energy Environ. Sci.* **2012**, *5*, 7943.

[29] A. M. Nardes, A. J. Ferguson, J. B. Whitaker, B. W. Larson, R. E. Larsen, M. Klára, P. A. Graf, O. V. Boltalina, S. H. Strauss and N. Kopidakis, *Adv. Funct. Mater.* **2012**, *22*, 4115.

[30] G. Zhao, Y. He and Y. Li, *Adv. Mater.* **2010**, *22*, 4355.

[31] M. Jørrgensen, J. E. Carlé, R. R. Søndergaard, M. Lauritzen, N. A. Dagnæs-Hansen, S. L. Byskov, T. R. Andersen, T. T. Larsen-Olsen, A. P. L. Böttiger, B. Andreasen, L. Fu, L. Zuo, Y. Liu, E. Bundgaard, X. Zhan, H. Chen and F. C. Krebs, *Sol. Energy Mater. Sol. Cells* **2013**, *119*, 84.

[32] A. K. Pandey, J. M. Nunzi, B. Ratier and A. Moliton, *Phys. Lett. A* **2008**, *372*, 1333.

[33] L. J. Rozanski, C. T. G. Smith, K. K. Gandhi, M. J. Beliatis, G. D. M. R. Dabera, K. D. G. I. Jayawardena, A. A. D. T. Adikaari, M. J. Kearney and S. R. P. Silva, *Sol. Energy Mater. Sol. Cells* **2014**, *130*, 513.

[34] F. L. M. Sam, M. A. Razali, K. D. G. I. Jayawardena, C. A. Mills, L. J. Rozanski, M. J. Beliatis and S. R. P. Silva, *Org. Electron.* **2014**, *15*, 3492.

[35] L. Hu, R. Cui, H. Huang, G. Lin, X. Guo, S. Yang, Y. Lian, J. Dong and B. Sun, *J. Nanosci. Nanotechnol.* **2015**, *15*, 5285.

[36] W. W. H. Wong, J. Subbiah, J. M. White, H. Seyler, B. Zhang, D. J. Jones and A. B. Holmes, *Chem. Mater.* **2014**, *26*, 1686.

[37] F. Zhao, X. Meng, Y. Feng, Z. Jin, Q. Zhou, H. Li, L. Jiang, J. Wang, Y. Li and C. Wang, *J. Mater. Chem. A* **2015**, *3*, 14991.

[38] B. Zhang, J. Subbiah, D. J. Jones and W. W. H. Wong, *Beilstein J. Org. Chem*. **2016**, *12*, 903.

[39] K. K. Gandhi, A. Nejim, M. J. Beliatis, C. A. Mills, S. J. Henley and S. R. P. Silva, *J. Photon. Energy* **2015**, ***5***, 057007.

[40] S. Han, Z. Fei, K. D. G. I. Jayawardena, M. J. Beliatis, Y.-B. Hahn, A. A. D. T. Adikaari, M. J. Heeney and S. R. P. Silva, *Thin Solid Films* **2015**, *576*, 38.

[41] K. D. G. I. Jayawardena, L. J. Rozanski, C. A. Mills, M. J. Beliatis, N. A. Nismy and S. R. P. Silva, *Nanoscale* **2013**, *5*, 8411.

[42] M. J. van Eis, R. J. Alvarado, L. Echegoyen, P. Seiler and F. Diederich, *Chem. Commun.* **2000**, *19*, 1859.

[43] V. S. P. K. Neti, M. R. Ceron, A. Duarte-Ruiz, M. M. Olmstead, A. L. Balch and L. Echegoyen, *Chem. Commun.* **2014**, *50*, 10584.

[44] R. Tao, T. Umeyama, T. Higashino, T. Koganezawa and H. Imahori, *Chem. Commun.* **2015**, *51*, 8233.

[45] B. Zhang, J. Subbiah, Y.-Y. Lai, J. M. White, D. J. Jones and W. W. H. Wong, *Chem. Commun.* **2015**, *51*, 9837.

[46] B. Zhang, J. M. White, D. J. Jones and W. W. H. Wong, *Org. Biomol. Chem.* **2015**, *13*, 10505.

[47] X. Meng, G. Zhao, Q. Xu, Z. a. Tan, Z. Zhang, L. Jiang, C. Shu, C. Wang and Y. Li, *Adv. Funct. Mater.* **2014**, *24*, 158.

[48] F. Steiner, S. Foster, A. Losquin, J. Labram, T. D. Anthopoulos, J. M. Frost and J. Nelson, *Mater. Horiz.* **2015**, *2*, 113.

[49] C. Koidis, S. Logothetidis, S. Kassavetis, C. Kapnopoulos, P. G. Karagiannidis, D. Georgiou and A. Laskarakis, *Sol. Energy Mater. Sol. Cells* **2013**, *112*, 36.

[50] S. T. Turner, P. Pingel, R. Steyrleuthner, E. J. W. Crossland, S. Ludwigs and D. Neher, *Adv. Funct. Mater.* **2011**, *21*, 4640.

[51] H. G. T. G.E. Irene, *Handbook of Ellipsometry*, William Andrew Publishing, Norwich, NY **2005**.

[52] D. Georgiou, A. Laskarakis, M. Morana, P. G. Karagiannidis and S. Logothetidis, *Sol. Energy Mater. Sol. Cells* **2014**, *125*, 190.

[53] S. Logothetidis, *Thin Films Handbook: Processing, Characterization and Properties*, Academic Press **2001**.

[54] W.-P. Wu, L.-L. Deng, X. Li and Y. Zhao, *Sci. Bull.* **2016**, *61*, 139.

[55] E. Chibowski and R. Perea-Carpio, *Adv. Colloid. Interface Sci.* **2002**, *98*, 245.

[56] C. M. Cardona, W. Li, A. E. Kaifer, D. Stockdale and G. C. Bazan, *Adv. Mater.* **2011**, *23*, 2367.